ACS Catalysis

Research Article

pubs.acs.org/acscatalysis

Design of Base Zeolite Catalysts by Alkali-Metal Grafting in Alcoholic Media

Tobias C. Keller, Kartikeya Desai, Sharon Mitchell, and Javier Pérez-Ramírez*

Institute for Chemical and Bioengineering, Department of Chemistry and Applied Biosciences, ETH Zurich, Vladimir-Prelog-Weg 1, CH-8093 Zurich, Switzerland

Supporting Information

ABSTRACT: This study investigates the synthesis of base catalysts through the postsynthetic grafting of alkali cations (Li, Na, K, Rb, or Cs) onto USY zeolites in alcoholic solutions of the corresponding metal hydroxides. In contrast to previous studies conducted in aqueous media, the utilization of alcohols (MeOH, EtOH, or *i*PrOH) offers increased control over the metalation process while simultaneously averting degradation and dissolution of the crystalline framework. The achievement of close to an atomic dispersion of the alkali metals in the zeolite is confirmed by in-depth characterization combining ^{23}Na MAS NMR, microscopy, elemental mapping, and CO_2 chemisorption. Both the size of the alkali cation and the carbon number of the alcohol influence the incorporation efficiency, which is found to correlate with the expected basic strength of the corresponding metal alkoxide. The presence of framework aluminum results in higher sodium loadings due to the parallel incorporation by both ion exchange and metalation. However, cations exchanged to the Al sites do not provide the distinct basic properties of the grafted metals, and thus, high-silica zeolites attain the highest basicity. Catalytic testing in the self-condensation of propanal, a model reaction for the deoxygenation of bio-oil, demonstrates excellent activity, with a > 90% selectivity to the aldol reaction and a stable performance. The selective character arising from the distinctive strength coupled with the isolated nature and high accessibility of the grafted basic sites holds a large potential for the development of superior zeolite catalysts for base-catalyzed applications.

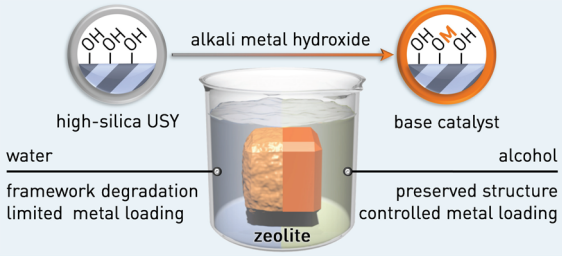

KEYWORDS: *basic zeolites, metal grafting, alkaline treatment, aldol condensation, bio-oil upgrading*

1. INTRODUCTION

Since the first applications of zeolite catalysts in the chemical industry, their unpaired success, for example, in petrochemical applications, has relied on postsynthetic modifications.[1−4] Intense efforts have resulted in a toolbox of simple and scalable treatments, which enable the precise tailoring of the active site and pore structure of a zeolite.[5,6] An important discovery, which has greatly expanded the versatility of zeolite catalysts, was the effectiveness of alkaline treatments to develop auxiliary mesoporosity in bulk zeolite crystals via desilication.[7−9] This enabled the alleviation of mass-transfer and accessibility constraints in numerous reactions, consequently enhancing the catalytic performance.[10−12] Based on the preferential dissolution of silicon over other metals in the zeolite, it was found that the addition of tri- or tetravalent cations to the alkaline solutions could be used to introduce metals into zeolites that evidence distinct properties from those deposited by traditional ion exchange or impregnation routes. For example, in the cases of Sn or Ga, this method provided an alternative to hydrothermal syntheses to generate sites that exhibited a tetrahedral coordination, and the associated highly selective Lewis acidity, as evidenced in the isomerization of sugar-based molecules.[13−15]

A fact that was only recently appreciated is that metalation phenomena can occur in the presence of basic salts alone (e.g., NaOH).[16] The deprotonation of silanol groups at high pH enables them to coordinate the cations (e.g., Na^+) from the solution, originating basic sites of moderate strength (Scheme 1). USY zeolites metalated in this way were shown to combine excellent selectivity with resistance to coking in the self-condensation of propanal and are thus attractive alternatives to traditional base catalysts such as alkali metal-exchanged zeolites (e.g., Cs-X) or alkaline earth metal oxides (e.g., MgO)[17] that suffer from quick deactivation due to their poor selectivity. To date, research efforts have primarily focused on high-silica zeolites to exclude catalytic side effects originating from the presence of aluminum.[18] However, this poses challenges due to the susceptibility of siliceous materials to dissolution and amorphization under basic conditions. The latter processes can be prevented through the application of certain additives, such as tetrapropylammonium (TPA^+) salts that stabilize the zeolite during the treatment.[18] However, the competitive interaction of the additives with the zeolite surface hampers the incorporation of alkali metals, thus limiting the maximum possible loading. Consequently, as illustrated in Scheme 1, alternative approaches to stabilize the zeolite framework under basic

Received: April 12, 2015
Revised: August 4, 2015
Published: August 4, 2015

DOI: 10.1021/acscatal.5b00761
ACS Catal. 2015, 5, 5388−5396

Scheme 1. Strategies to Graft Basic Sites on Zeolites by Treatment with Alkali Metal (M) Hydroxides and the Impact on Key Structural Variables[a]

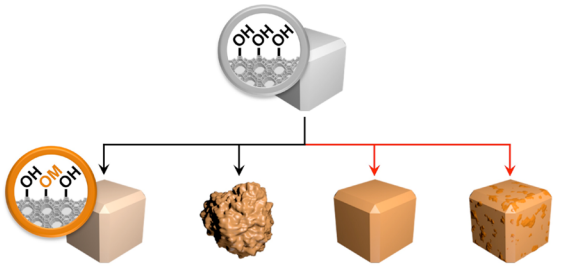

Media	water + TPA$^+$	water	methanol ethanol	isopropanol
Base strength	low (carbonate)	any	high (hydroxide)	high (hydroxide)
Metal loading	+	++	++	+++
Crystallinity	preserved	amorphized	preserved	amorphized
Side effects	none	dissolution	none	cluster formation

[a]The novel approaches described in this contribution are highlighted with red arrows.

conditions appear highly desirable to facilitate the synthesis and further enhance the activity of these materials in base-catalyzed reactions.

In the past, base treatments have been carried out predominantly in aqueous media, which is indeed the ideal choice if mesopore formation by demetalation is targeted.[5] However, if the ultimate goal is metal grafting, rather than dissolution, the utilization of organic solvents such as alcohols could represent a simple approach to preserve the textural properties of a zeolite while allowing the incorporation of high metal loadings. The nonaqueous solvents impede the hydrolysis of Si−O bonds and thus reduce their reactivity,[19] a strategy that was previously exploited for the grafting of Al and Sn onto mesoporous silicas.[20,21]

This contribution tackles the design of basic USY zeolites via the base-assisted grafting of alkali metals in alcoholic media of different polarity. The concentration, strength, and location of the resulting basic sites are characterized as a function of the type and amount of alkali metal and the concentration of aluminum in the starting zeolite. Subsequent evaluation in the gas-phase condensation of propanal, which is investigated as model reaction for bio-oil deoxygenation,[22,23] demonstrates the excellent performance of catalysts displaying isolated metal centers of moderate strength.

2. EXPERIMENTAL SECTION

2.1. Catalyst Preparation. The high-silica USY zeolite was obtained in protonic form from Tosoh Corporation (HSZ-390HUA, Si/Al = 405, denoted "SiUSY"), and Al-containing counterparts were purchased in protonic form from Zeolyst (CBV720, Si/Al = 15, denoted "AlUSY15"; CBV760, Si/Al = 30, denoted "AlUSY30"). Amorphous SiO_2 (silica gel, high purity grade) was obtained from Sigma-Aldrich. The as-received samples were denoted with the suffix "-ar". For the grafting of alkali metals, the as-received zeolite (2 g) was introduced into a solution (60 cm^3) of the desired concentration (0−0.2 M) of alkali metal hydroxide (LiOH, ABCR, 98%; NaOH, Sigma-Aldrich, 97%; KOH, Fisher Chemicals, 85%; RbOH·$2H_2O$, Fluka, 95%; CsOH 50 wt % in H_2O, ABCR, 99.9%) in the selected solvent (H_2O; methanol, Sigma-Aldrich, 99.8%; ethanol, Sigma-Aldrich, 99.9%; isopropanol, Fluka, 99.9%) at room temperature, stirred at 500 rpm for 10 min, filtered, washed thoroughly with the same solvent (3 times with ca. 100 cm^3), and dried at 65 °C. Samples treated at 0 M represent blank experiments to study the impact of the treatment in the alcohol alone. Catalysts prepared with NaOH were subsequently calcined in static air (550 °C, 5 h, ramp rate of 5 °C min^{-1}). To facilitate the discussion, catalysts treated at 0.1 M NaOH in methanol are coded with the suffix "-Na" throughout the manuscript. The metal was also incorporated into the zeolite by dry impregnation. For this purpose, an aqueous solution (1.16 g) of sodium nitrate (0.75 M $NaNO_3$, Sigma-Aldrich, 99.5%) was added dropwise to the zeolite (1 g). The catalysts were dried and calcined as described above.

2.2. Catalyst Characterization. Nitrogen sorption at −196 °C was carried out in a Micromeritics TriStar II instrument. Prior to the measurement, the samples were evacuated at 300 °C for 3 h. Powder X-ray diffraction (XRD) was measured in a PANalytical X'Pert PRO-MPD diffractometer with Bragg−Brentano geometry using Ni-filtered Cu Kα radiation (λ = 0.1541 nm). The patterns were recorded in the 2θ range of 5−70° with an angular step size of 0.05° and a counting time of 8 s per step. The relative crystallinity of the samples was determined following ASTM standard D3906. The Na and Li content in the solids was determined by inductively coupled plasma optical emission spectroscopy (ICP-OES) using a Horiba Ultima 2 instrument equipped with photomultiplier tube detection against a 5-point calibration curve. Samples (0.1 g) were dissolved in mixtures of hydrofluoric acid (3 cm^3, 48 wt % in H_2O, Sigma-Aldrich) and aqua regia (0.5 cm^3), followed by the addition of a saturated solution of boric acid (50 cm^3, Sigma-Aldrich, 99.5%) and water (45 cm^3). X-ray fluorescence (XRF) was conducted with an EDAX Orbis Micro-XRF analyzer equipped with a Rh source operated at a voltage of 20 kV and a current of 500 μA. ^{23}Na magic angle spinning nuclear magnetic resonance (MAS NMR) spectra were recorded at 185.2 MHz using 4 mm ZrO_2 rotors at a spinning speed of 10 kHz on a Bruker Avance 700 spectrometer. Spectra were obtained using 2048 accumulations with a pulse length of 1 μs, a recycle delay of 1 s, and solid NaCl (Sigma, 99.9%) as a reference (δ = 7.21 ppm). Prior to analysis, the samples were dried in vacuum. Scanning electron microscopy (SEM) was performed on Zeiss Gemini 1530 FEG at 5 kV. Scanning transmission electron (STEM) micrographs in bright-field (BF) and high-angle annular dark-field (HAADF) modes, as well as energy dispersive X-ray spectroscopy (EDS) element maps were acquired on a FEI Talos instrument operated at 200 kV. This instrument is equipped with a high-brightness Schottky FEG and a SuperX EDS system which includes four silicon drift detectors symmetrically placed around the sample that detect over a solid angle of 0.9 sr, enabling efficient chemical imaging at zero degree tilt. The samples were dispersed as dry powders onto lacey-carbon-coated copper grids. As zeolites are known to be gradually amorphized under prolonged exposure to electron radiation, the mapping experiments were typically performed with beam currents of around 70 pA and with a dwell time of 10 ms to further protect the specimen. HAADF images were acquired before and after EDS measurements to corroborate the absence of major morphological changes due to beam damage. Temperature-programmed desorption of carbon dioxide (CO_2-TPD) and ammonia (NH_3-TPD) were carried out in a Micromeritics Autochem II chemisorption analyzer coupled with a MKS Cirrus 2 quadrupole mass spectrometer. For CO_2-

DOI: 10.1021/acscatal.5b00761
ACS Catal. 2015, 5, 5388−5396

TPD, the catalyst (0.1 g) was pretreated in He flow (20 cm^3 min^{-1}) at 550 °C for 2 h. Afterward, CO_2 (50 pulses, 1 cm^3) diluted in He flow (10 cm^3 min^{-1}) was adsorbed at 50 °C, followed by He purging at the same temperature for 60 min. CO_2 desorption was monitored in the range of 50−700 °C (heating rate of 10 °C min^{-1}). The procedure used to determine the number of weak basic sites is detailed in Figure S1. For NH_3-TPD, the catalyst (0.1 g) was pretreated in He flow (30 cm^3 min^{-1}) at 550 °C for 2 h. Afterward, 10 vol % of NH_3 in He (30 cm^3 min^{-1}) was adsorbed three times at 200 °C for 30 min, followed by He purging at the same temperature for 60 min. NH_3 desorption was monitored in the range of 200−700 °C (heating rate of 10 °C min^{-1}).

2.3. Catalytic Testing. The self-condensation of propanal was evaluated at atmospheric pressure in a continuous-flow fixed-bed reactor (12 mm internal diameter). The catalyst (0.3 g, 0.2−0.4 mm particle size) was pretreated in He (50 cm^3 min^{-1}) at 450 °C for 1 h prior to the reaction. Propanal (99%, Acros Organics) was fed to the tubular reactor using a Chemyx Fusion 100 Classic syringe pump (1.2 cm^3 h^{-1}) via a vaporization line heated to 150 °C using He (50 cm^3 min^{-1}) as carrier gas. The reactions were conducted at 400 °C for 2−10 h, and the products were analyzed by an online HP Agilent 6890 gas chromatograph equipped with a flame ionization detector (FID) and a capillary HP-5 column. Conversion (X) and product yields (Y) were calculated based on the integrated peak area of the component of interest, normalized to the total FID response. Reaction rates were determined by normalizing the amount of propanal converted per hour to the amount of catalyst, or the amount of alkali metal in the catalyst, respectively. The former was determined on the basis of the average conversion measured between 90 and 120 min on stream.

3. RESULTS AND DISCUSSION

The Results and Discussion are divided into four parts. Section 3.1 investigates the influence of an aqueous and alcoholic solvent on the stability of high-silica zeolites during alkaline treatment. In Sections 3.2 and 3.3, respectively, the effects of the cationic size and of the Al content of the zeolites are examined. The catalytic performance of the basic zeolites is evaluated and rationalized on the basis of the properties evidenced in Section 3.4. For all catalysts, the treatment conditions, along with the resulting textural properties and composition are summarized in Table S1.

3.1. Stability of USY Zeolites in Alkaline Media. To assess the relative stability in alcoholic and aqueous base media, we treated a high-silica USY zeolite (SiUSY, Si/Al = 405) with 0.1 M NaOH in binary mixtures of water and methanol. This zeolite was selected for two reasons: to maximize its susceptibility to the alkaline treatment and to facilitate the characterization due to the absence of alkali metals in cation exchange positions associated with framework aluminum. As expected,[18] the sample treated in pure water experienced severe textural modification (Figure S2), induced by the complete amorphization of the zeolite framework. The micropore volume was reduced by 60%, and an increased N_2 uptake in the range of p/p_0 = 0.1−0.5 provided evidence for the formation of small mesopores (Figure 1a). With increasing methanol content of the treatment solution, the changes in the porosity and crystallinity are gradually reduced, whereas the properties of the starting zeolite remain fully preserved if the amount of H_2O in the solution is less than 20 wt %. Simultaneously, the yield of solids increased from 71% in water to 97% in the case of methanol, confirming that not only the amorphization but also the dissolution of the zeolite can be prevented through the utilization of alcoholic solvents.

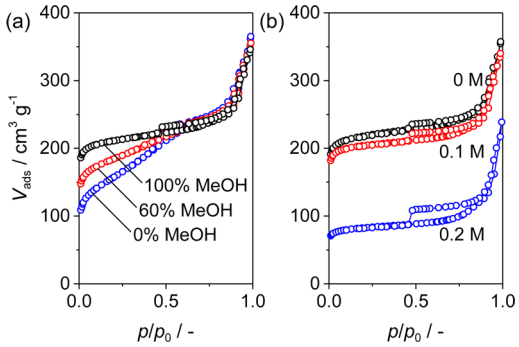

Figure 1. N_2 sorption isotherms of SiUSY zeolites NaOH-treated (a) in 0.05 M solutions in binary mixtures of H_2O:MeOH and (b) at different concentrations in MeOH.

Having demonstrated the improved stability of zeolites in alcohols, we studied the relationship between the concentration of the base, the selection of the solvent, and the resulting sodium loading. For this purpose, the SiUSY zeolite was subjected to treatments in the range of 0−0.2 M NaOH in methanol. The resulting textural properties are summarized in Figure 2, whereas representative N_2 isotherms and X-ray diffractograms are provided in Figures 1b and S3, respectively. The crystallinity and microporosity are fully preserved in most cases, but the external surface area drops with increasing alkalinity to ca. 50% of its initial value. Up to 2 wt % of sodium can be incorporated, more than double the value previously attained in aqueous media.[18] Although characterization of the samples before and after calcination typically yielded identical results, it appears that too high metal loadings can reduce the thermal stability of the materials: The sample prepared at c_{NaOH} = 0.2 M evidenced a partial amorphization of the framework during the calcination step that is confirmed by the reduced N_2 uptake (Figure 1b). We realized during the course of this study that the calcination step conveys no catalytic benefits and can thus be omitted for the investigated reaction. Nevertheless, it is a possible issue that needs to be monitored for other potential applications. For the sample treated at c_{NaOH} = 0.1 M, SEM imaging revealed that the crystal morphology was preserved (Figure 3a,b), although slight surface roughening was evidenced. Complementary investigation by HAADF-STEM, coupled with EDX analysis, indicated that the sodium was homogeneously distributed over the zeolite crystals, suggesting a high dispersion of the alkali metal (Figures 3c,d and S4). This implies that the alkali metal is not only grafted to silanol groups on the external surface, but also to internal defects.

Comparatively, the utilization of alcohols of higher carbon number such as ethanol and isopropanol led to the notably increased introduction of sodium (up to 5.4 wt % for the sample prepared at 0.1 M NaOH in isopropanol) with respect to that achieved in methanol, but at the cost of larger alterations of the textural properties and crystallinity (Figure 2). Comparison of the metal incorporation efficiency revealed that the type of solvent has a stronger impact than the base concentration. For example, less than 10% of the alkali metal present in a 0.05 M NaOH solution is incorporated into the zeolite if methanol is used as the solvent. In the case of ethanol, this value increases to ca. 60%; whereas in the case of

DOI: 10.1021/acscatal.5b00761
ACS Catal. 2015, 5, 5388−5396

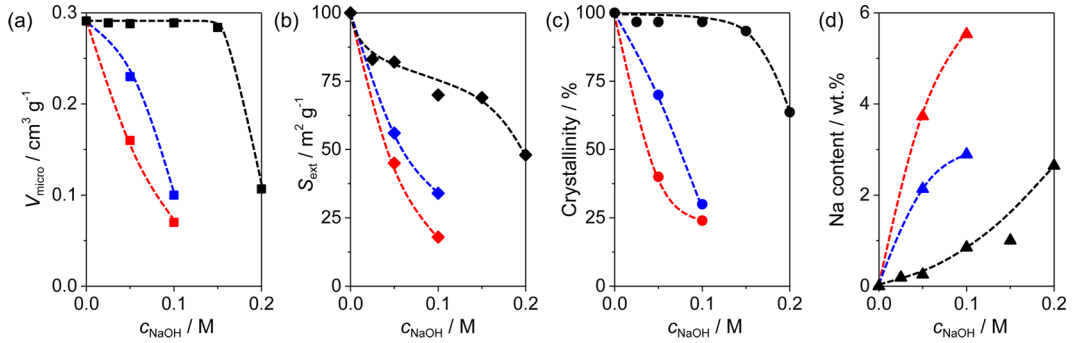

Figure 2. (a) Micropore volume, (b) external surface area, (c) crystallinity, and (d) sodium content of NaOH-treated SiUSY zeolites as a function of the base concentration in MeOH (black), EtOH (blue), and *i*PrOH (red).

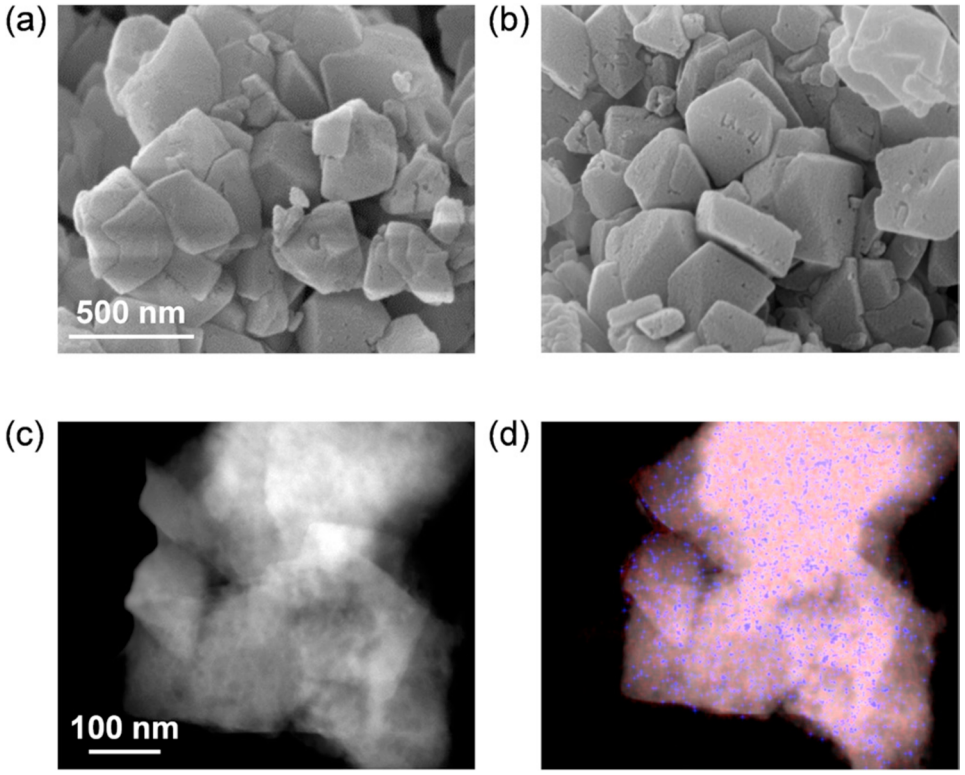

Figure 3. SEM images of the (a) as-received and (b) NaOH-treated (0.1 M in MeOH) SiUSY zeolite. The corresponding (c) HAADF-STEM image, and (d) elemental map of Si (pink) and Na (blue) in the NaOH-treated sample. The scale bars apply to both images in the same row.

isopropanol, the complete incorporation of the alkali metal is observed. This trend likely results from the different basicity of the corresponding alkoxides: Upon dissolution in an alcohol, NaOH is expected to be almost fully converted to the corresponding metal alkoxide.[24,25] The basic strength of alkoxides increases with the number of carbon atoms.[26,27] Furthermore, longer-chain alcohols enable the presence of stronger bases due to the reduced leveling effect (the conjugated acid of a solvent is the strongest base that can exist in the respective medium). As silanol groups do not have a uniform acid strength, but exhibit an acidity distribution due to the different site geometries,[28,29] a larger fraction can be irreversibly deprotonated and coordinate metal cations in the presence of stronger bases.

To benchmark the base-assisted metalation with conventional methods for the introduction of metals, a sample with a sodium content of 2 wt % was prepared by dry impregnation. This loading is comparable to the samples prepared with 0.2 M NaOH in methanol and 0.05 M NaOH in ethanol. Although the latter two samples retained a crystallinity of approximately 70%, the comparative crystallinity of the dry-impregnated sample was only 30% after calcination, and the porous properties were reduced by a similar extent (Table S1).

The chemical environment of the sodium atoms was investigated by ^{23}Na MAS NMR. A single contribution, whose intensity increases with the sodium loading, was evidenced around δ = −1.8 ppm for all uncalcined samples (Figure 4a). Accordingly, the chemical environment of the grafted sodium is independent of the metal loading. For samples with sodium loadings <2 wt %, this signal is largely preserved after calcination (Figure 4b), indicating that the grafted sites are thermally stable. The only changes evident are a slightly lowered chemical shift and a second contribution centered at δ = 7 ppm, which is indicative of minor restructuring (Figure 4b). In contrast, samples with reduced crystallinity (e.g., the ones attained in ethanol and isopropanol)

DOI: 10.1021/acscatal.5b00761
ACS Catal. 2015, 5, 5388−5396

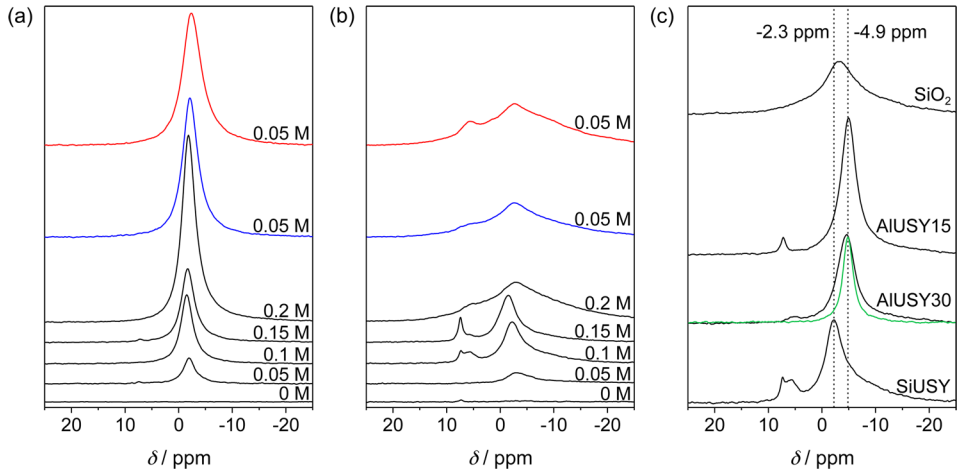

Figure 4. ^{23}Na MAS NMR spectra of (a) uncalcined and (b) calcined SiUSY zeolites NaOH-treated at different concentrations in MeOH (black), EtOH (blue), and *i*PrOH (red). (c) ^{23}Na MAS NMR spectra of aluminosilicates NaOH-treated at 0.1 M in MeOH (black) and ion-exchanged to the Na^+ form (green).

evidence a very broad signal around $\delta = -2.6$ ppm, consistent with the loss of the uniform geometry delivered by the crystalline framework and the agglomeration of the sodium cations into denser phases. The basic properties of the materials were assessed by CO_2-TPD (Figure 5). It is important to note

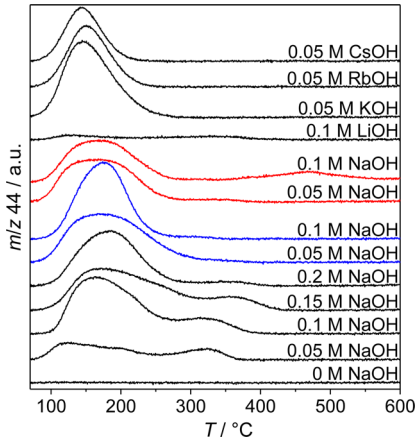

Figure 5. CO_2-TPD profiles of SiUSY zeolites treated with various alkali metal hydroxides in MeOH (black), EtOH (blue), and *i*PrOH (red) at different concentrations.

that even though the samples were outgassed in situ prior to the analysis, water was evolved simultaneously during CO_2 desorption. This water likely originates from surface rearrangements, and thus, a CO_2-specific detector (e.g., MS) should be used instead of an unselective one (e.g., a thermal conductivity detector). The zeolite treated in the absence of alkali metals shows no significant desorption, confirming the negligible basicity of the high-silica framework. On the other hand, two major contributions were observed for samples containing alkali metals, centered around 180 and 320 °C, respectively. The relative amounts of weak and strong basic sites were determined from the amount of CO_2 desorbed between 100−280 °C, and above 280 °C, respectively, as described in Figure S1. For the samples in which the textural properties were preserved, both weak and strong basic sites can be observed. With increasing sodium loading, these contributions become more pronounced, and the peak maxima shift toward higher temperatures. In contrast, the partially amorphized samples only evidence the contribution at low temperature, indicating that both a high metal loading and crystallinity are essential to maximize the total concentration of basic sites. The amount of weak basic sites correlates linearly with the sodium content if no degradation occurs (Figure 6), but the incorporation of additional sodium does not result in increased basicity if the crystallinity is compromised.

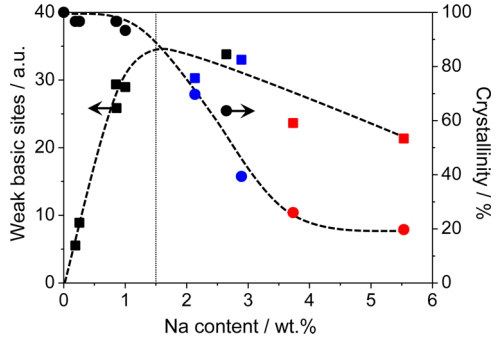

Figure 6. Relative amount of weak basic sites (squares) and crystallinity (circles) of NaOH-treated SiUSY zeolites prepared in MeOH (black), EtOH (blue), and *i*PrOH (red) as a function of the sodium content.

3.2. Impact of the Cation Size. The basic properties of alkali-exchanged zeolites are known to depend strongly on the cation size, where larger cations are typically associated with the development of stronger sites due to their lower Sanderson electronegativity.[30] The occurrence of similar effects for metalated base centers seems plausible and thus deserves investigation. Accordingly, Li^+, K^+, Rb^+, and Cs^+ were grafted on the USY zeolite by treatment with the corresponding metal hydroxide (c_{MOH} = 0.025−0.1 M) in methanol. The potassium-loaded sample prepared with 0.05 M KOH displayed a 5-fold increase in the metal-to-silicon ratio compared to the sodium containing counterpart, and the values evidenced upon treatment with CsOH or RbOH are approximately 8 times higher (Figure 7). The increased efficiency in the incorporation of larger metals can be explained by the stronger basicity of the corresponding alkoxides due to the larger size of the cation,

DOI: 10.1021/acscatal.5b00761
ACS Catal. 2015, 5, 5388−5396

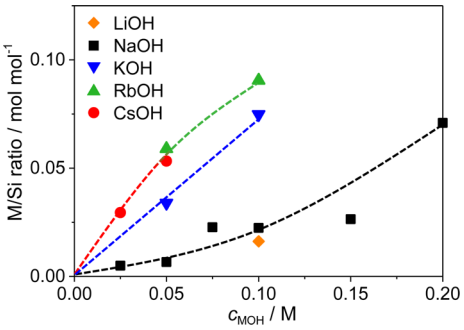

Figure 7. Metal-to-silicon ratio in alkali metal hydroxide-treated SiUSY zeolites as a function of the base concentration in MeOH.

confirming the observations made for the NaOH-grafted samples that the basic strength of the alkoxides in the solution determines the incorporation efficiency. Accordingly, as not only the molar loading, but also the weight of the individual cation increases, the employed concentration needs to be reduced compared to the NaOH treatment if a preservation of the porous properties is desired (Table S1). The catalysts treated with the large cations evidence a higher CO_2 desorption compared to the sodium-derived samples (Figure 5). The highest number of mild basic sites was attained for KOH or RbOH-treated samples, whereas the structural damage to the Cs-catalysts resulted in a lower number of basic sites. The catalyst prepared with LiOH incorporated ca. 30% less cations than its NaOH-treated counterpart, which makes sense based on its smaller cation size. However, it evidences almost no interaction with CO_2, indicating that either very few basic sites are generated in the presence of LiOH or that they are very weak.

Compared with the Na-metalated samples, the larger ionic radii (0.133 and 0.147 nm with respect to 0.097 nm) and the higher atomic weight (39.10 and 85.47 amu with respect to 22.9 amu) of potassium and rubidium should facilitate the microscopic observation of small metal nanoparticles or clusters formed in zeolites, as they become progressively larger than the point resolution limit of the microscope (ca. 0.25 nm) and enable a stronger phase (Z-) contrast, respectively. Examination of the Rb- and K-metalated zeolites confirms the high dispersion of the alkali metals over the zeolite crystals (Figures 8 and S5), in agreement with the observations for the Na-metalated samples. In particular, the absence of features exhibiting strong Z-contrast in the BF or HAADF (high-angle annular dark-field)-STEM suggests a near atomic dispersion of the grafted alkali metals, strongly supporting the indications from other techniques as CO_2-TPD. It is noteworthy that the visualization of very small metal clusters or atomically dispersed metal centers in zeolites is highly challenging, and to the best of our knowledge, for zeolite Y, this has so far only been achieved by a single work in the presence of large iridium cations (ionic radius of 0.200 nm).[31] The respective presence of rubidium or potassium throughout the samples is confirmed by chemical mapping in STEM mode. The preserved crystallinity of the zeolite support is evidenced by the lattice fringes seen in the lower magnification bright field (BF) image of the RbOH-treated SiUSY sample. Finally, the images also highlight the complex morphology of the zeolite particles, revealing the presence of mesopores within the structure. It is expected that the alkali metals coordinate not only at the external surface, but simultaneously also at other internal defects such as mesopores and silanol nests originating from the steaming and subsequent dealumination treatments employed during the synthesis of USY zeolites.

3.3. Role of Aluminum and Support. For simplicity, research on the generation of basic sites by metalation has so far been limited to highly siliceous zeolites, leaving the role of aluminum unclear. Furthermore, it was not known whether the protocols developed for the postsynthetic grafting of basic sites would also be effective for nonzeolitic supports such as silica, which would be an attractive economical alternative. To tackle these critical points, we have treated two USY zeolites with higher Al contents (AlUSY30, Si/Al = 30 and AlUSY15, Si/Al = 15), as well as an amorphous SiO_2 sample, with 0.1 NaOH in methanol. Herein, the as-received samples (protonic form) were denoted "-ar", whereas the base-treated catalysts were denoted "-Na". Similar to the high-silica zeolite sample, no

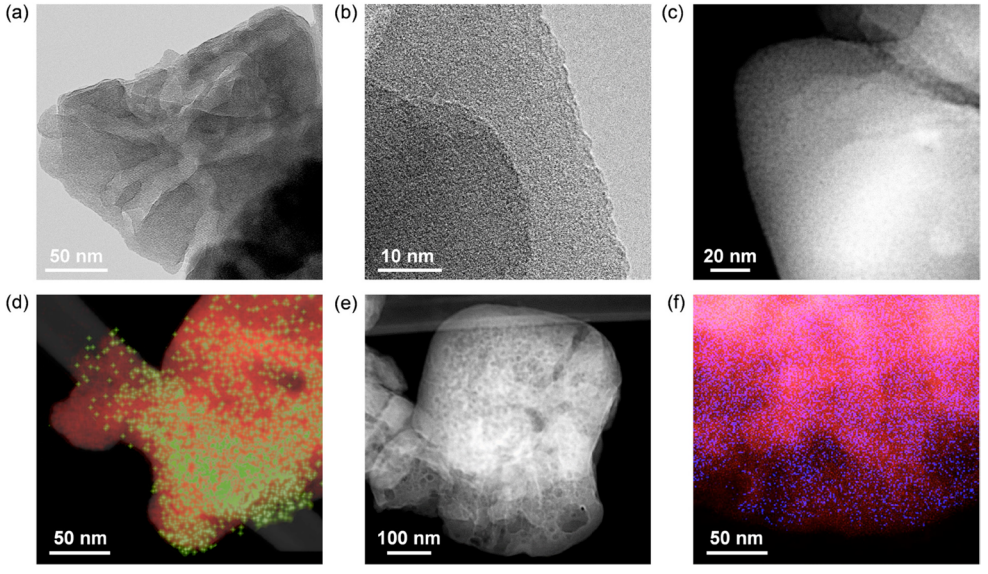

Figure 8. (a,b) HRTEM, (c) HAADF-STEM, and (d) elemental map of Si (red) and Rb (green) in the RbOH-treated SiUSY zeolite (0.05 M in MeOH). (e) HAADF-STEM and (f) elemental map of Si (red) and K (blue) for the KOH-treated analogue (0.05 M in MeOH).

DOI: 10.1021/acscatal.5b00761
ACS Catal. 2015, 5, 5388−5396

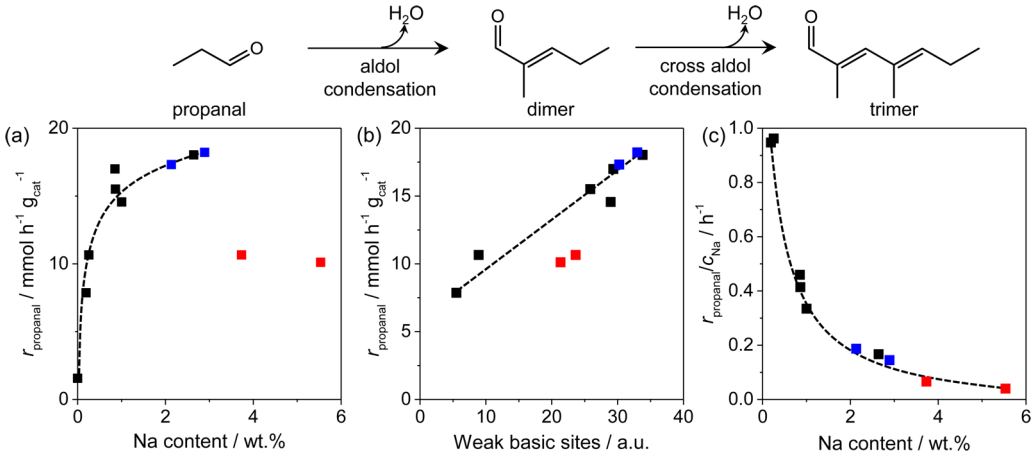

Figure 9. Rate of propanal conversion as a function of the (a) sodium content and (b) the relative amount of weak basic sites in SiUSY zeolites prepared by alkaline treatment in methanol (black), ethanol (blue), and isopropanol (red). (c) Rate per mole of sodium in the zeolite as a function of the Na content over the same catalysts.

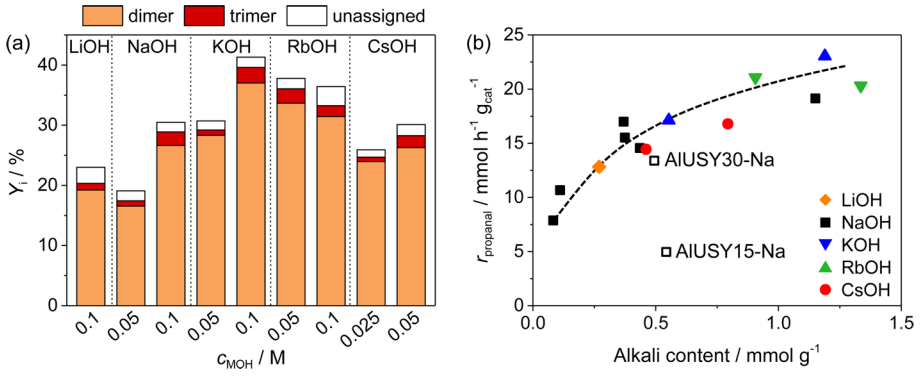

Figure 10. (a) Product yields and (b) rate of propanal conversion obtained in the self-condensation over SiUSY zeolites alkaline-treated in MeOH with different metals and concentrations. The open symbols in (b) represent the values obtained over NaOH-treated AlUSY zeolites.

significant changes in the textural properties were observed under these conditions (Table S1). The amount of sodium incorporated increases with the aluminum content, reaching 1.12 wt % in AlUSY30 and 1.26 wt % AlUSY15 compared with 0.85 wt % in the SiUSY zeolite.

Analyses by ^{23}Na MAS NMR evidence a dominant contribution at δ = −2.3 ppm (Figure 4c) in the calcined SiUSY-Na sample, whereas the signals of both AlUSY samples are centered around δ = −4.9 ppm. The different chemical environment can be readily assigned to sodium cations in ion exchange positions by comparison with the as-received AlUSY30-ar sample after ion-exchange with $NaNO_3$ at neutral pH (green trace in Figure 4c), which should not evidence any alkali metal cations grafted to deprotonated silanol groups. Accordingly, the increased sodium loading of the aluminum-containing zeolites results from the preferential incorporation into cation exchange sites balancing the negative framework charge in these materials, while only a minor amount of Na is introduced by grafting. Comparison of the basicity of the USY zeolites by CO_2-TPD supports this observation (Figure S6), as the AlUSY zeolites evidence much lower concentrations of basic sites than their SiUSY counterpart despite their higher sodium content. The ion-exchange of the acid sites can also be followed by the temperature-programmed desorption of ammonia (NH_3-TPD) (Figure S7). In the (as-received) protonic form, both AlUSY zeolites evidence a distribution of mild and strong acid sites that is typical of USY zeolites,[32] but after the treatment, no peak is detected anymore in the NH_3 desorption profile. Accordingly, a better approach to graft basic sodium onto Al-containing zeolites could be to first ion-exchange it with the desired cation at neutral pH before the base treatment is carried out.

The surface area of the SiO_2 sample was already reduced by one-third after a mild treatment in 0.1 M NaOH in MeOH. In contrast to the zeolites, the Si-atoms are not confined in a crystalline framework and are thus more reactive. This also resulted in the incorporation of 10% more sodium compared to the SiUSY treated under identical conditions (Table S1). ^{23}Na MAS NMR spectra evidence a single broad signal at δ = −2.6 ppm (Figure 4c), similar to that observed in the SiUSY catalysts treated in ethanol and isopropanol, which suffered from partial amorphization.

3.4. Catalytic Evaluation. The catalytic performance of the basic zeolites was investigated in the gas-phase self-condensation of propanal (Figure 9). Recently, such reactions have received significant interest as model systems for the catalytic deoxygenation of crude bio-oil.[16,18,33−35] Catalytic deoxygenation treatments applied to pyrolysis vapors are highly interesting, as they could reduce the hydrogen consumption in a subsequent hydrodeoxygenation step while simultaneously shifting the average chain length of the obtained hydrocarbons toward the desired gasoline and diesel fractions.[22,23] The metalated high-silica zeolites all exhibited approximately a 90% selectivity to the aldol condensation pathways. The main

DOI: 10.1021/acscatal.5b00761
ACS Catal. 2015, 5, 5388−5396

product was the aldol condensation dimer, although increasing yields of trimers became evident at higher conversions. In agreement with previous observations,[18] the catalytic performance remained stable over the 2 h time-on-stream. The product distributions obtained over the NaOH-derived samples are detailed in the Supporting Information (Figure S8); the most active sample was attained via a treatment in 0.2 M NaOH. Consistent with the indications of CO_2-TPD, the catalytic activity of the sodium−metalated SiUSY zeolites cannot be explained solely on the basis of the amount of metal incorporated (Figure 9a). In contrast, the rate of propanal conversion is found to correlate linearly with the relative amount of weak basic sites determined in the samples (Figure 9b). The only outliers are the partially degraded samples attained in isopropanol, which likely contain side-phases that form carbonates during CO_2-TPD, and thus overestimate the active site number. These observations confirm the detrimental influence of the structural degradation of the zeolites observed at higher metal loadings. In fact, the reduced utilization of sodium in these samples becomes clear on comparison of the variation in the rate of propanal conversion per mole of sodium in the zeolite, which drops sharply as a function of the sodium loading (Figure 9c). This indicates that the maximum loading of alkali metal is limited by the need to ensure the generation of isolated sites in a crystallographically well-defined sample.

Interestingly, very similar product distributions were evidenced upon evaluation of the zeolites metalated with different alkali metals (Figure 10a). The Li-loaded sample was slightly less active than its Na-containing counterpart, which is in agreement with the 30% lower metal content, but comes unexpectedly considering the low CO_2 uptake of the sample. This is likely the result of a weak interaction between the Li^+ cations and the CO_2 that consequently leads to an underestimation of the number of basic sites in the material and highlights the problems of CO_2-TPD for the assessment of solid bases.[16,36,37] Ideally, this technique is only used to compare materials of similar nature, and changing the cation in a zeolite can already lead to difficulties in the interpretation.[36] Instead, the alkali metal content can be used as a rough descriptor, provided that the textural properties of the samples are comparable (Figure 10b). It appears that the type of alkali metal only has a minor influence on the site utilization, as the observed trend is valid for all of the cations. Comparatively, the treatments with 0.1 M KOH and 0.1 M RbOH in methanol yielded the most active catalysts, which reach yields of aldol condensation products approaching 40% (almost 10% higher than those achieved over the sodium−metalated samples). These materials also evidenced a remarkably stable performance over 10 h time-on-stream (Figure S9).

Evaluation of the USY zeolites with higher Al contents revealed that the as-received catalysts exhibited an equivalently high activity to that of the sodium−metalated SiUSY zeolite (Figure 11). However, as the strong acid sites of these catalysts favor dehydration, cracking, and aromatization reactions,[33] they result in a poor selectivity, with a less than 2% yield of the aldol condensation products. Furthermore, because these pathways are accompanied by coke formation, the rate of propanal conversion dropped more quickly with increasing aluminum content (Figure S10). Upon base-assisted metalation, the catalytic activity of both AlUSY30-Na and AlUSY15-Na was reduced below the level attained for SiUSY-Na, whereas the selectivity to the aldol condensation is substantially increased and the rate of propanal conversion remained stable over 2 h

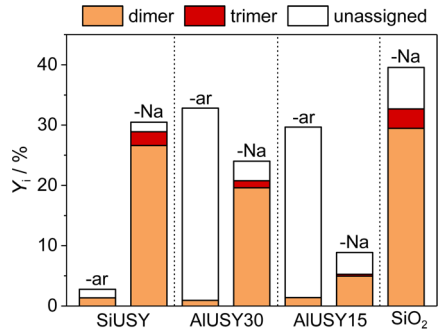

Figure 11. Product yields obtained in the self-condensation of propanal over the different USY zeolites and amorphous SiO_2 in as-received (ar) and NaOH-treated (0.1 M in MeOH) forms.

on stream. As for the lithium-containing sample, the high activity of these zeolites following alkaline treatment cannot be explained based on the relative concentration of basic sites evidenced by CO_2-TPD. Possibly, the presence of residual acid sites in close proximity to the generated basic sites favors a bifunctional acid−base reaction pathway and thus ensures a high turnover frequency. Although in the investigated reaction, the high-silica zeolite remains the optimal catalyst, the possibility to graft selective basic sites on aluminum-containing zeolites expands the versatility of the method and may be exploited in more advanced ways in the future (e.g., for tandem catalysis).

The SiO_2−Na catalyst attained a high catalytic activity (Figure 11) that was slightly lower than the most active zeolites. However, the selectivity to the aldol condensation products (S_{aldol} = 82%) was ca. 10% lower than over the zeolite samples, which likely results from the more heterogeneous distribution of active sites in the sample. Nevertheless, the results highlight the facile extrapolation of the developed insights to other silica-based materials such as other zeolite frameworks, or mesostructured silicas.

4. CONCLUSIONS

The utilization of alcoholic solvents for the generation of basic sites in zeolites by alkaline treatments widens the range of achievable metal loadings while preventing the dissolution or amorphization of the zeolite in a simple manner, without the need of organic additives. This strategy could also be extended to amorphous silicas that would otherwise dissolve rapidly upon alkaline treatment. For a given concentration of the alkali metal hydroxide, the amount of grafted species was found to correlate with the expected strength of the corresponding alkali metal alkoxide, increasing with the size of the alkali metal cation (Cs > Rb > K > Na > Li) and the carbon number of the alcohol applied (C3 > C2 > C1). Correspondingly, in the case of sodium, alcohols with higher carbon numbers enabled a better control over the metal loading, whereas in the case of potassium, rubidium, or cesium, methanol was found to be optimal. The presence of aluminum in the zeolite favors the incorporation of alkali metals. However, the amount of basic sites does not increase proportionally, as the cations are preferentially incorporated by ion exchange rather than grafting. Extensive characterization coupled with evaluation in the gas-phase condensation of propanal demonstrated the need to ensure the generation of isolated basic sites of mild strength while preserving the crystallinity of the zeolite to attain highly active, selective, and stable catalysts. The advantage of applying

DOI: 10.1021/acscatal.5b00761
ACS Catal. 2015, 5, 5388−5396

basic over acidic zeolites was clearly evidenced by the rapid deactivation and significantly reduced yields of the aldol condensation products observed over the latter. Nevertheless, the alkaline treatment of the aluminum-containing USY zeolites in alcohols improved their selectivity and stability, although the performance of the high-silica analogue remained superior.

■ ASSOCIATED CONTENT

Supporting Information

The Supporting Information is available free of charge on the ACS Publications website at DOI: 10.1021/acscatal.5b00761.

Characterization of selected samples by N_2 sorption, X-ray diffraction, microscopy, CO_2-TPD, and NH_3-TPD. Details on the method for the determination of the number of weak basic sites. Product distribution and stability tests over the zeolites (PDF)

■ AUTHOR INFORMATION

Corresponding Author

*E-mail: jpr@chem.ethz.ch. Phone: +41-44-633-7120.

Notes

The authors declare no competing financial interest.

■ ACKNOWLEDGMENTS

This work was funded by ETH (research grant ETH-31 13-1) and the European Union Seventh Framework Programme (FP7/2007−2013) under grant agreement no. 604307. The Scientific Center for Optical and Electron Microscopy (ScopeM) at ETH Zurich is thanked for use of the facilities and Dr. Fabian Gramm for assistance with imaging. We thank Elodie G. Rodrigues and Begoña Puértolas for experimental input.

■ REFERENCES

(1) Corma, A. *Chem. Rev.* **1997**, *97*, 2373−2420.
(2) Kühl, G. H. In *Catalysis and Zeolites − Fundamentals and Applications*; Weitkamp, J., Puppe, L., Eds.; Springer: Berlin, 1999; pp 81−197.
(3) Biswas, J.; Maxwell, I. E. *Appl. Catal.* **1990**, *63*, 197−258.
(4) Primo, A.; Garcia, H. *Chem. Soc. Rev.* **2014**, *43*, 7548−7561.
(5) Valtchev, V.; Majano, G.; Mintova, S.; Pérez-Ramírez, J. *Chem. Soc. Rev.* **2013**, *42*, 263−290.
(6) Mahmoud, E.; Lobo, R. F. *Microporous Mesoporous Mater.* **2014**, *189*, 97−106.
(7) Ogura, M.; Shinomiya, S.; Tateno, J.; Nara, Y.; Nomura, M.; Kikuchi, E.; Matsukata, M. *Appl. Catal., A* **2001**, *219*, 33−43.
(8) Verboekend, D.; Pérez-Ramírez, J. *Catal. Sci. Technol.* **2011**, *1*, 879−890.
(9) Serrano, D. P.; Escola, J. M.; Pizarro, P. *Chem. Soc. Rev.* **2013**, *42*, 4004−4035.
(10) Holm, M. S.; Taarning, E.; Egeblad, K.; Christensen, C. H. *Catal. Today* **2011**, *168*, 3−16.
(11) Chen, L.-H.; Li, X.-Y.; Rooke, J. C.; Zhang, Y.-H.; Yang, X.-Y.; Tang, Y.; Xiao, F.-S.; Su, B.-L. *J. Mater. Chem.* **2012**, *22*, 17381−17403.
(12) Yan, Y.; Guo, X.; Zhang, Y.; Tang, Y. *Catal. Sci. Technol.* **2015**, *5*, 772−785.
(13) Dijkmans, J.; Gabriëls, D.; Dusselier, M.; de Clippel, F.; Vanelderen, P.; Houthoofd, K.; Malfliet, A.; Pontikes, Y.; Sels, B. F. *Green Chem.* **2013**, *15*, 2777−2785.
(14) Dapsens, P. Y.; Menart, M. J.; Mondelli, C.; Pérez-Ramírez, J. *Green Chem.* **2014**, *16*, 589−593.
(15) Dapsens, P. Y.; Mondelli, C.; Jagielski, J.; Hauert, R.; Pérez-Ramírez, J. *Catal. Sci. Technol.* **2014**, *4*, 2302−2311.
(16) Keller, T. C.; Isabettini, S.; Verboekend, D.; Rodrigues, E. G.; Pérez-Ramírez, J. *Chem. Sci.* **2014**, *5*, 677−684.
(17) Climent, M. J.; Corma, A.; Iborra, S.; Velty, A. *J. Mol. Catal. A: Chem.* **2002**, *182−183*, 327−342.
(18) Keller, T. C.; Rodrigues, E. G.; Pérez-Ramírez, J. *ChemSusChem* **2014**, *7*, 1729−1738.
(19) Morris, R. E.; Weigel, S. J. *Chem. Soc. Rev.* **1997**, *26*, 309−317.
(20) Mokaya, R.; Jones, W. *J. Mater. Chem.* **1999**, *9*, 555−561.
(21) Ryoo, R.; Jun, S.; Kim, J. M.; Kim, M. J. *Chem. Commun.* **1997**, 2225−2226.
(22) Mortensen, P. M.; Grunwaldt, J. D.; Jensen, P. A.; Knudsen, K. G.; Jensen, A. D. *Appl. Catal., A* **2011**, *407*, 1−19.
(23) Graça, I.; Lopes, J. M.; Cerqueira, H. S.; Ribeiro, M. F. *Ind. Eng. Chem. Res.* **2013**, *52*, 275−287.
(24) Caldin, E. F.; Long, G. *Nature* **1953**, *172*, 583−584.
(25) Caldin, E. F.; Long, G. *J. Chem. Soc.* **1954**, 3737−3742.
(26) Hine, J.; Hine, M. *J. Am. Chem. Soc.* **1952**, *74*, 5266−5271.
(27) Bowden, K. *Chem. Rev.* **1966**, *66*, 119−131.
(28) Nawrocki, J. *J. Chromatogr. A* **1997**, *779*, 29−71.
(29) Kondo, J. N.; Yoda, E.; Ishikawa, H.; Wakabayashi, F.; Domen, K. *J. Catal.* **2000**, *191*, 275−281.
(30) Barthomeuf, D. *Microporous Mesoporous Mater.* **2003**, *66*, 1−14.
(31) Ortalan, V.; Uzun, A.; Gates, B. C.; Browning, N. D. *Nat. Nanotechnol.* **2010**, *5*, 506−510.
(32) Niwa, M.; Suzuki, K.; Isamoto, K.; Katada, N. *J. Phys. Chem. B* **2006**, *110*, 264−269.
(33) Shen, W.; Tompsett, A. A.; Xing, R.; Conner, W. C., Jr.; Huber, G. W. *J. Catal.* **2012**, *286*, 248−259.
(34) Zhu, X.; Lobban, L. L.; Mallinson, R. G.; Resasco, D. E. *J. Catal.* **2010**, *271*, 88−98.
(35) Hoang, T. Q.; Zhu, X.; Sooknoi, T.; Resasco, D. E.; Mallinson, R. G. *J. Catal.* **2010**, *271*, 201−208.
(36) Barthomeuf, D. *Catal. Rev.: Sci. Eng.* **1996**, *38*, 521−612.
(37) Auroux, A.; Gervasini, A. *J. Phys. Chem.* **1990**, *94*, 6371−6379.

DOI: 10.1021/acscatal.5b00761
ACS Catal. 2015, 5, 5388−5396